Chemical Engineering Journal 95 (2003) 67–81

Chemical Engineering Journal

www.elsevier.com/locate/cej

Simulation study of a dense polymeric catalytic membrane reactor with plug–flow pattern

José M. Sousa [a,b], Adélio Mendes [b,*]

[a] *Departamento de Química, Apartado 202, Universidade de Trás-os-Montes e Alto Douro, 5001-911 Vila-Real Codex, Portugal*

[b] *LEPAE—Departamento de Engenharia Química, Faculdade de Engenharia, Universidade do Porto, Rua Roberto Frias, 4200-465 Porto, Portugal*

Received 22 October 2002; accepted 17 March 2003

Abstract

A theoretical study on a tubular membrane reactor, assuming isothermal operation, plug–flow pattern and using a dense polymeric catalytic membrane, is performed. The reactor conversion for an $A \rightleftarrows B$ equilibrium gas-phase reaction is analyzed, considering the influence of the reactants and products diffusion and sorption coefficients, the influence of the total pressure gradient and the influence of the ratio between the membrane thickness and its internal radius as well as the influence of the feed location (tube side or shell side) and the co-current, counter-current and cross-flow operation modes. One of the most unexpected conclusion is that for a set of conditions where the co-current and counter-current flows leads to differences in the reactor performance, the co-current flow is always better than the counter-current flow, exactly the reverse of what takes place when the membrane performs only gas separation. It is also concluded that the relative permeate pressure favors or penalizes the conversion, depending on the relative permeabilities of each reaction component. It is also concluded that the best reactor's feed location and the optimum r^t/δ ratio depend on the relative sorption and diffusion coefficients of the reaction components as well as on the range of the Thiele modulus and contact time operation values.

Keywords: Dense polymeric catalytic membrane; Plug–flow pattern reactor; Gas-phase reaction; Equilibrium reaction; Modeling

1. Introduction

The drive towards greater economic and environmental efficiency has resulted in the development of more environmentally friendly processes, when compared with the existing technology. An innovation in the recent investigation has been to create synergy through combined catalytic and separation technologies. Catalytic membrane reactor operation is a typical example of such synergistic combination, with several reactor configurations proposed and extensively reviewed [1–3]. Among others, it can be referred the so-called "catalytic membrane reactor" (CMR), where the membrane is simultaneously permselective and catalytic, and the "packed bed membrane reactor" (PBMR), where the membrane is permselective but not catalytic.

The main objective of such an investigation has been to achieve some conversion enhancement over the thermodynamic equilibrium value, but other promising advantages are being studied [4], namely catalytic membrane reactors with segregated feed of reactants to improve safety and selectivity [5–7] and inert membranes for distributed feed of reactants along the reactor length in PBMR, to improve selectivity and stability [8–11]. In particular, dehydrogenation reactions with metallic (palladium or palladium alloys) [12–15], ceramic [16–18], and composite [19–21] membranes are the most common examples of the conversion enhancement, with hydrogen being selectively removed. Shifting the thermodynamic equilibrium in this way has obvious industrial interest. It allows for reduced reaction temperatures, thereby minimizing side reactions and heating costs. Also, both reaction and separation may be achieved in a single unit, making the membrane reactor a very cost-effective unit operation.

Most of the nowadays discussed reactions susceptible to be carried out in membrane reactors are in the high temperature range and, sometimes, in chemical aggressive environments, so it is not surprising that polymeric membranes have hardly ever been used, except in biocatalysis. However, they have attracted an increasing interest in the last few years, as they present some advantages over inorganic membranes [2,22,23]. Besides, polymeric membranes can be easily produced with incorporated catalysts (nano-sized dispersed metallic clusters [24,25], zeolites and activated carbons [26] or metallic complexes [27–29]) and can be easily made in different forms (flat, tubes, tubules, hollow fibres

* Corresponding author. Tel.: +351-22-508-1695; fax: +351-22-508-1449.
E-mail address: mendes@fe.up.pt (A. Mendes).

1385-8947/$ – see front matter © 2003 Elsevier Science B.V. All rights reserved.
doi:10.1016/S1385-8947(03)00083-4

Nomenclature

D_i	diffusion coefficient of the component i (m^2/s)
D_{ref}	diffusion coefficient of the reference component (component A) (m^2/s)
f	variable related with the operation mode ($f = 1$ for co-current; $f = -1$ for counter current)
H_i	Henry's sorption coefficient of the component i (mol/(m^3 Pa))
H_{ref}	Henry's sorption coefficient of the reference component (component A) (mol/(m^3 Pa))
j	variable related with the feed location ($j = 0$ for tube side feed; $j = 1$ for shell side feed)
k_d	direct reaction rate constant (s^{-1})
K_e	reaction equilibrium constant
L	length of the reactor (m)
p_i	partial pressure of species i in equilibrium with the sorbed concentration (Pa)
p_i^F	partial pressure of component i in the feed stream (Pa)
p_i^P	partial pressure of component i in the permeate stream (Pa)
p_i^R	partial pressure of component i in the retentate stream (Pa)
P_{ref}	reference pressure (feed pressure) (Pa)
P^F	total pressure in the feed (Pa)
P^P	total pressure in the permeate side (Pa)
P^R	total pressure in the retentate side (Pa)
Q_{ref}	reference volumetric flowrate (feed volumetric flowrate) (m^3/s)
Q^F	total feed volumetric flowrate (m^3/s)
Q^P	total permeate volumetric flowrate (m^3/s)
Q^R	total retentate volumetric flowrate (m^3/s)
r	membrane radial coordinate (m)
r^P	membrane radius on the permeate side (m)
r^R	membrane radius on the retentate side (m)
r^s	external membrane radius (shell side) (m)
r^t	internal membrane radius (tube side) (m)
R	local reaction rate (mol/(m^3 s))
$\Re$	universal gas constant (Pa m^3/(mol K))
T	absolute temperature (K)
x_B	molar fraction of component B
X_A	reactor conversion of reactant A
X_A^E	thermodynamic equilibrium conversion of reactant A, based on the feed conditions
z	tube/shell axial coordinate (m)

Greek symbols

α_i	dimensionless diffusion coefficient of the component i
χ_A	relative conversion (X_A/X_A^E)
δ	membrane thickness (m)
Φ	Thiele modulus $\delta(k_d/D_{ref})^{1/2}$
γ_i	dimensionless sorption coefficient of the component i
Γ	dimensionless contact time ($(2\pi r^t L D_{ref} H_{ref} \Re T)/\delta Q_{ref}$)
Γ_{MC}	dimensionless contact time for the maximum conversion
Γ_{TPC}	dimensionless contact time for the total permeation condition
λ	dimensionless axial coordinate
ν_i	stoichiometric coefficient of the component i ($\nu_A = -1$, $\nu_B = 1$)
Θ	relative reaction coefficient ($((\gamma_B \Psi_B)/(\gamma_A \Psi_A))/K_e$
ρ	dimensionless membrane spatial coordinate
Ψ_i	dimensionless partial pressure of species i in equilibrium with the sorbed concentration
Ψ^P	dimensionless total pressure in the permeate side
Ψ^R	dimensionless total pressure in the retentate side
Ψ_i^F	dimensionless partial pressure of component i in the feed
Ψ_i^P	dimensionless partial pressure of component i in the permeate stream
Ψ_i^R	dimensionless partial pressure of component i in the retentate stream
ζ^P	dimensionless total permeate volumetric flowrate
ζ^R	dimensionless total retentate volumetric flowrate

and spiral wound) [1,28,30]. The ability of these materials to be, in some way, tailored to the needs makes them very promising for future applications.

As a consequence of these developments, there is a growing need for effective theoretical models that can help understanding the potentialities and the limitations of polymeric membrane reactors, leading to optimized designs. There are in the open literature several studies about modeling membrane reactors, although only a few actually deal with CMR's (where the catalyst is either the membrane itself, or it is incorporated in the porous membrane structure or membrane surface, or it is occluded inside the membrane) [2,6,31–36]. To the best of our knowledge and beyond our recent work [32,33], only a few researchers [31,34,35] modeled polymeric catalytic membrane reactors, however, for conducting liquid phase reactions and considering mixed flow pattern in both sides.

In a recent theoretical study [32,33], we analyzed the performance of a dense polymeric catalytic membrane reactor when running an equilibrium reaction. The model considered assumes perfectly mixed flow pattern in both retentate and permeate sides, flat membrane and isothermal

operation. In the present work, we will consider a tubular membrane reactor with plug–flow pattern in both retentate and permeate sides. We chose a hypothetical equilibrium reaction A⇄B, where A and B can embrace more than one reactant–product, because the proposed model has an analytical solution for the membrane mass balance equations, thus allowing for a more accurate and faster solution of the global model and without compromising the main conclusions. We will analyze the influence of some parameters and operation modes on the reactor's conversion, such as the sorption and diffusion coefficients of the reaction components, pressure difference through the membrane, reactor's configuration with respect to the flow patterns (co-current, counter-current and cross-flow), tube side or shell side feed location and ratio between the tube radius and the membrane thickness.

2. Model development

Fig. 1 represents a sketch of the catalytic membrane reactor considered in the present study. It consists of a tube and shell chambers at different (but constant) total pressures P^{T} and P^{S}, respectively, separated by a catalytic membrane of thickness δ filled with a hypothetical nano-sized catalyst homogeneously distributed throughout it. A reaction of the type A⇄B is considered. This figure shows a reactor fed from the tube side and operating in co-current flow. However, models considering a reactor fed from the shell side and the operation modes in counter-current and cross-flow are also considered in the present study. The proposed models are based on the following main assumptions:

1. Steady state and isothermal operation.
2. Negligible film transport resistance.
3. The flow pattern for the retentate and permeate streams (co- and counter-current flows) is considered to be plug flow.
4. Negligible pressure's drop along the retentate and permeate sides.
5. Fickian transport through the membrane.
6. Sorption equilibrium between the bulk gas phase and the membrane surface described by Henry's law.
7. Constant diffusion and sorption coefficients.
8. Elementary reaction mechanism.
9. Homogeneous catalyst distribution through the membrane.
10. The reaction occurs only on the catalyst nanoparticles surface.
11. Equal concentration on the catalyst surface and in the polymer matrix (any relationship could be considered in principle, but this one simplifies the original problem without compromising the conclusions).

The mathematical model comprises the steady state mass balance equations for the membrane and for the retentate and permeate sides as well as the respective boundary conditions.

2.1. Partial and total mass balances in the retentate side

$$\frac{1}{\Re T}\frac{\mathrm{d}(Q^{\mathrm{R}}p_i^{\mathrm{R}})}{\mathrm{d}z} - 2\pi r^{\mathrm{R}}\, D_i H_i \frac{\mathrm{d}p_i}{\mathrm{d}r}\bigg|_{r=r^{\mathrm{R}},z} = 0, \quad i = \mathrm{A}, \mathrm{B} \tag{1}$$

$$\frac{P^{\mathrm{R}}}{\Re T}\frac{\mathrm{d}Q^{\mathrm{R}}}{\mathrm{d}z} - 2\pi r^{\mathrm{R}}\sum_i D_i H_i \frac{\mathrm{d}p_i}{\mathrm{d}r}\bigg|_{r=r^{\mathrm{R}},z} = 0, \quad i = \mathrm{A}, \mathrm{B} \tag{2}$$

The respective boundary conditions are as follows: $z = 0$ $p_i^{\mathrm{R}} = p_i^{\mathrm{F}}$ and $Q^{\mathrm{R}} = Q^{\mathrm{F}}$.

2.2. Partial and total mass balances in the permeate side

For co- and counter-current flows, the equations are as follows:

$$\frac{1}{\Re T}\frac{\mathrm{d}(Q^{\mathrm{P}}p_i^{\mathrm{P}})}{\mathrm{d}z} + f2\pi r^{\mathrm{P}}\, D_i H_i \frac{\mathrm{d}p_i}{\mathrm{d}r}\bigg|_{r=r^{\mathrm{P}},z} = 0, \quad i = \mathrm{A}, \mathrm{B} \tag{3}$$

$$\frac{P^{\mathrm{P}}}{\Re T}\frac{\mathrm{d}Q^{\mathrm{P}}}{\mathrm{d}z} + f2\pi r^{\mathrm{P}}\sum_i D_i H_i \frac{\mathrm{d}p_i}{\mathrm{d}r}\bigg|_{r=r^{\mathrm{P}},z} = 0, \quad i = \mathrm{A}, \mathrm{B} \tag{4}$$

$f = 1$ or $f = -1$ according to the flow it is either in co- or counter-current, respectively. The respective boundary conditions for co-current flow are as follows:

$$z = L, \quad \left(\frac{\mathrm{d}p_i^{\mathrm{P}}}{\mathrm{d}z}\right) = 0 \quad \text{and} \quad z = 0, \quad Q^{\mathrm{P}} = 0.$$

For counter-current flow, the same boundary conditions are applied, however, at opposite ends.

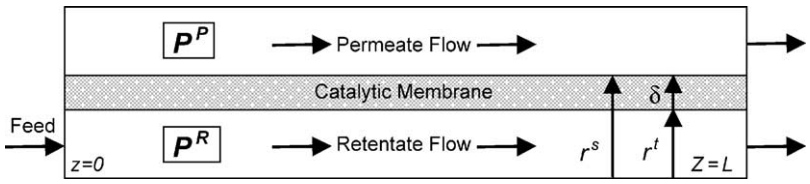

Fig. 1. Schematic diagram of the dense polymeric catalytic tubular membrane reactor (for co-current flow and tube side feed).

For cross-flow operation mode, the composition on the permeate side at each axial coordinate is considered to be the result of the permeation rate of the various species [37]:

$$p_i^{\mathrm{P}}(z) = \frac{D_i H_i (\mathrm{d}p_i/\mathrm{d}r)|_{r=r^{\mathrm{P}},z}}{\sum_i D_i H_i (\mathrm{d}p_i/\mathrm{d}r)\big|_{r=r^{\mathrm{P}},z}} P^{\mathrm{P}} \tag{5}$$

The volumetric flow rate for this arrangement is given by (it is indifferent the flow direction):

$$\frac{P^{\mathrm{P}}}{\Re T} Q^{\mathrm{P}}(z) + 2\pi r^{\mathrm{P}} \sum_i D_i H_i \frac{\mathrm{d}p_i}{\mathrm{d}r}\bigg|_{r=r^{\mathrm{P}},z} = 0 \tag{6}$$

2.3. Mass balance in the membrane

$$D_i H_i \left(\frac{\mathrm{d}^2 p_i}{\mathrm{d}r^2} + \frac{1}{r}\frac{\mathrm{d}p_i}{\mathrm{d}r} \right) + \nu_i R = 0, \quad i = \mathrm{A}, \mathrm{B} \tag{7}$$

where R is the local reaction rate:

$$R = k_{\mathrm{d}} \left(H_{\mathrm{A}} p_{\mathrm{A}} - \frac{H_{\mathrm{B}} p_{\mathrm{B}}}{K_{\mathrm{e}}} \right) \tag{8}$$

The corresponding boundary conditions for Eq. (7) are as it follows:

For tube side feed : $r = 0, \quad p_i = p_i^{\mathrm{R}}(z); \quad r = \delta, \quad p_i = p_i^{\mathrm{P}}(z)$

For shell side feed : $r = 0, \quad p_i = p_i^{\mathrm{P}}(z); \quad r = \delta, \quad p_i = p_i^{\mathrm{R}}(z)$

The variables p_i^{F}, p_i^{R} and p_i^{P} represent the partial pressure of species i in feed, retentate and permeate streams, respectively; p_i is the partial pressure of species i in equilibrium with the sorbed concentration; P^{F}, P^{R} and P^{P} are the total pressures of the feed, retentate and permeate streams, respectively; Q^{F}, Q^{R} and Q^{P} the total volumetric flowrate of the feed, retentate and permeate streams, respectively. $\Re$ is the universal gas constant and T the absolute temperature. $r^{\mathrm{R}} = r^{\mathrm{t}}$ and $r^{\mathrm{P}} = r^{\mathrm{s}}$ for tube side feed; $r^{\mathrm{R}} = r^{\mathrm{s}}$ and $r^{\mathrm{P}} = r^{\mathrm{t}}$ for shell side feed, where r^{t} is the internal membrane radius (tube side) and r^{s} the external membrane radius (shell side); r the radial coordinate perpendicular to the membrane surface; z the axial coordinate along the reactor length; L the length of the reactor and δ the membrane thickness. D_i and H_i are the diffusion and sorption coefficients of component i; ν_i is the stoichiometric coefficient of component i ($\nu_{\mathrm{A}} = -1$, $\nu_{\mathrm{B}} = 1$); k_{d} the direct reaction rate constant and K_{e} the reaction equilibrium constant.

In dimensionless form, the Eqs. (1)–(7) become as follows:

$$\frac{\mathrm{d}(\zeta^{\mathrm{R}}\Psi_i^{\mathrm{R}})}{\mathrm{d}\lambda} - \left(1 + \frac{\delta}{r^{\mathrm{t}}}\right)^{j} \Gamma\, \alpha_i \gamma_i \frac{\mathrm{d}\Psi_i}{\mathrm{d}\rho}\bigg|_{\rho=j,\lambda} = 0, \quad i = \mathrm{A}, \mathrm{B} \tag{9}$$

$$\Psi^{\mathrm{R}} \frac{\mathrm{d}\zeta^{\mathrm{R}}}{\mathrm{d}\lambda} - \left(1 + \frac{\delta}{r^{\mathrm{t}}}\right)^{j} \Gamma \sum_i \alpha_i \gamma_i \frac{\mathrm{d}\Psi_i}{\mathrm{d}\rho}\bigg|_{\rho=j,\lambda} = 0, \quad i = \mathrm{A}, \mathrm{B} \tag{10}$$

$$\lambda = 0, \quad \Psi_i^{\mathrm{R}} = \Psi_i^{\mathrm{F}} \quad \text{and} \quad \zeta^{\mathrm{R}} = 1$$

$$\frac{\mathrm{d}\left(\zeta^{\mathrm{P}}\Psi_i^{\mathrm{P}}\right)}{\mathrm{d}\lambda} + f\left(1 + \frac{\delta}{r^{\mathrm{t}}}\right)^{1-j} \Gamma\, \alpha_i \gamma_i \frac{\mathrm{d}\Psi_i}{\mathrm{d}\rho}\bigg|_{\rho=1-j,\lambda} = 0, \quad i = \mathrm{A}, \mathrm{B} \tag{11}$$

$$\Psi^{\mathrm{P}} \frac{\mathrm{d}\zeta^{\mathrm{P}}}{\mathrm{d}\lambda} + f\left(1 + \frac{\delta}{r^{\mathrm{t}}}\right)^{1-j} \Gamma \sum_i \alpha_i \gamma_i \frac{\mathrm{d}\Psi_i}{\mathrm{d}\rho}\bigg|_{\rho=1-j,\lambda} = 0, \quad i = \mathrm{A}, \mathrm{B} \tag{12}$$

$$\lambda = 1, \quad \frac{\mathrm{d}\Psi_i^{\mathrm{P}}}{\mathrm{d}\lambda} = 0 \quad \text{and} \quad \lambda = 0, \quad \zeta^{\mathrm{P}} = 0 \quad (\text{for } f = 1)$$

$$\Psi_i^{\mathrm{P}}(\lambda) = \frac{\alpha_i \gamma_i (\mathrm{d}\Psi_i/\mathrm{d}\rho)|_{\rho=1-j,\lambda}}{\sum_i \alpha_i \gamma_i (\mathrm{d}\Psi_i/\mathrm{d}\rho)|_{\rho=1-j,\lambda}} \Psi^{\mathrm{P}} \qquad i = \mathrm{A}, \mathrm{B} \tag{13}$$

$$\Psi^{\mathrm{P}}\zeta^{\mathrm{P}}(\lambda) + f\left(1 + \frac{\delta}{r^{\mathrm{t}}}\right)^{1-j} \Gamma \sum_i \alpha_i \gamma_i \frac{\mathrm{d}\Psi_i}{\mathrm{d}\rho}\bigg|_{\rho=1-j,\lambda} = 0, \quad i = \mathrm{A}, \mathrm{B} \tag{14}$$

$$\frac{\mathrm{d}^2\Psi_i}{\mathrm{d}\rho^2} + \frac{1}{\rho + r^{\mathrm{t}}/\delta}\frac{\mathrm{d}\Psi_i}{\mathrm{d}\rho} + \nu_i \frac{\Phi^2}{\alpha_i \gamma_i}\left(\gamma_{\mathrm{A}}\Psi_{\mathrm{A}} - \frac{\gamma_{\mathrm{B}}\Psi_{\mathrm{B}}}{K_{\mathrm{e}}}\right) = 0, \quad i = \mathrm{A}, \mathrm{B} \tag{15}$$

$\rho = j\,(\forall\lambda), \quad \Psi_i = \Psi_i^{\mathrm{R}}(\lambda)$ and

$\rho = 1 - j\,(\forall\lambda), \quad \Psi_i = \Psi_i^{\mathrm{P}}(\lambda)$

$j = 0$ for tube side feed and $j = 1$ for shell side feed, where

$$\Psi_i^{\mathrm{F}} = \frac{p_i^{\mathrm{F}}}{P_{\mathrm{ref}}} \qquad \Psi^{\mathrm{R}} = \frac{P^{\mathrm{R}}}{P_{\mathrm{ref}}} \qquad \Psi_i^{\mathrm{R}} = \frac{p_i^{\mathrm{R}}}{P_{\mathrm{ref}}} \qquad \Psi^{\mathrm{P}} = \frac{P^{\mathrm{P}}}{P_{\mathrm{ref}}}$$

$$\Psi_i^{\mathrm{P}} = \frac{p_i^{\mathrm{P}}}{P_{\mathrm{ref}}} \qquad \Psi_i = \frac{p_i}{P_{\mathrm{ref}}} \qquad \zeta^{\mathrm{R}} = \frac{Q^{\mathrm{R}}}{Q_{\mathrm{ref}}} \qquad \zeta^{\mathrm{P}} = \frac{Q^{\mathrm{P}}}{Q_{\mathrm{ref}}}$$

$$\rho = \frac{r - r^{\mathrm{t}}}{\delta} \qquad \lambda = \frac{z}{L} \qquad \alpha_i = \frac{D_i}{D_{\mathrm{ref}}} \qquad \gamma_i = \frac{H_i}{H_{\mathrm{ref}}}$$

$$\Phi = \delta\left(\frac{k_{\mathrm{d}}}{D_{\mathrm{ref}}}\right)^{1/2} \qquad \Gamma = \frac{2\pi r^{\mathrm{t}} L D_{\mathrm{ref}} H_{\mathrm{ref}} \Re T}{\delta Q_{\mathrm{ref}}}$$

The subscripts i and *ref* refer to the i-th and reference components and the superscripts F, R and P refer to the feed, retentate and permeate sides, respectively. Ψ is the dimensionless pressure, α represents the dimensionless diffusion coefficient, γ the dimensionless sorption coefficient, ζ the dimensionless flow rate, λ the dimensionless tube/shell axial coordinate and ρ the dimensionless membrane radial coordinate. Φ is the Thiele modulus (ratio between the characteristic diffusion time of the reference component and the characteristic reaction time of the direct reaction) and Γ the dimensionless contact time (ratio between the characteristic feed flow time and the characteristic permeation time of the reference component). Feed conditions are taken as the reference for P_{ref} and Q_{ref} Component A is taken as the reference for D_{ref} and H_{ref}.

The relative conversion, χ_{A}, is defined as the ratio between the conversion of reactant A, X_{A}, and the thermodynamic equilibrium conversion based on feed conditions, X_{A}^{e}, and is used to evaluate the membrane reactor performance. The reactor's conversion is calculated using the conventional equation:

$$X_{\text{A}} = 1 - \frac{\zeta^{\text{R}}\Psi_{\text{A}}^{\text{R}} + \zeta^{\text{P}}\Psi_{\text{A}}^{\text{P}}}{\zeta^{\text{F}}\Psi_{\text{A}}^{\text{F}}} \tag{16}$$

We still need to define the relative reaction coefficient, which measures how far the reaction is from the thermodynamic equilibrium:

$$\Theta = \frac{(\gamma_{\text{B}}\Psi_{\text{B}})/(\gamma_{\text{A}}\Psi_{\text{A}})}{K_{\text{e}}} \tag{17}$$

2.4. Solution strategy

The general strategy used for solving the model equations is the same as adopted before [32,33]: in order to overcome numerical instability problems, especially for counter-current flow and for high Thiele modulus values, a time derivative term was added to the right-hand side of Eqs. (9) and (11), transforming this problem into a pseudo-transient one. The composition on the permeate side for cross-flow operation mode (Eq. (13)) was calculated using a Newton–Raphson iterative scheme. The mass balance equations for the membrane (Eq. (15)) were solved analytically (see Appendix A); ζ^{R} and ζ^{P} from Eqs. (10) and (12) were computed using Simpson's rule. The partial differential equations resulting from (9) and (11) were spatially discretized using a tailor-made code based on finite differences. The time integration routine LSODA [38] was then used to integrate the resulting set of time dependent equations. The solution is considered to be in steady state when the time derivative of each dependent variable and for each of the spatial coordinate is smaller than a pre-defined value.

3. Results and discussion

A study on how the sorption and diffusion of the reaction components affects the reactor conversion as a function of the contact time (Γ) and Thiele modulus (Φ) values was done previously [39]. It was concluded that the reactor's conversion could be significantly enhanced if the diffusion coefficients of the reaction products are higher than the reactants ones and/or the sorption coefficients of the reactants are higher than the reaction products ones. In the present work, we will study the influence of other parameters and operation modes.

3.1. Influence of the reactants and products diffusion coefficients

Fig. 2 (upper part) shows the contact time at the total permeation condition (TPC), i.e. when the retentate flow is zero [39], as a function of the Thiele modulus and for different dimensionless diffusion coefficients of component B. Lower part shows the relative conversion of the reactor as a function of the Thiele modulus, for different dimensionless diffusion coefficients of component B and for different contact times. It is clear from these results that, for an intermediate range of Thiele moduli, the attainable conversion in the reactor could be far above the thermodynamic equilibrium value; the higher the diffusion coefficient of the reaction product, the higher is the reactor conversion (see Fig. 2, lower part). It can also be seen that the maximum conversion is attained at the TPC. Associated with this behavior, it can still be referred that, for a given set of diffusion coefficients, the contact time at the TPC decreases with the Thiele modulus and, for a given Thiele modulus value, it decreases with an increase of the diffusion coefficient of the reaction product (see Fig. 2, upper part). As the contact time is related with the reactor size, these results show that the reactor should operate for intermediate Thiele modulus values and for a ratio between the diffusion coefficient of the reaction product and the reactant as high as possible. The enhancement of the reactor conversion is due to the selective separation of the reaction product. For medium/high Thiele modulus values, this separation effect is offset, because the backward reaction rate overtakes the direct reaction rate [39].

3.2. Influence of the reactants and products sorption coefficients

Fig. 3 (lower part) shows the relative conversion of the reactor as a function of the Thiele modulus for different contact times and for different dimensionless sorption coefficients of component B. In the upper part, it is shown the contact time as function of the Thiele modulus values for the TPC and for the maximum of the conversion as a function of the Thiele modulus values. As it can be seen, the highest conversion is now achieved for $\Phi \to \infty$ and the conversion's enhancement improves inversely with the ratio between the

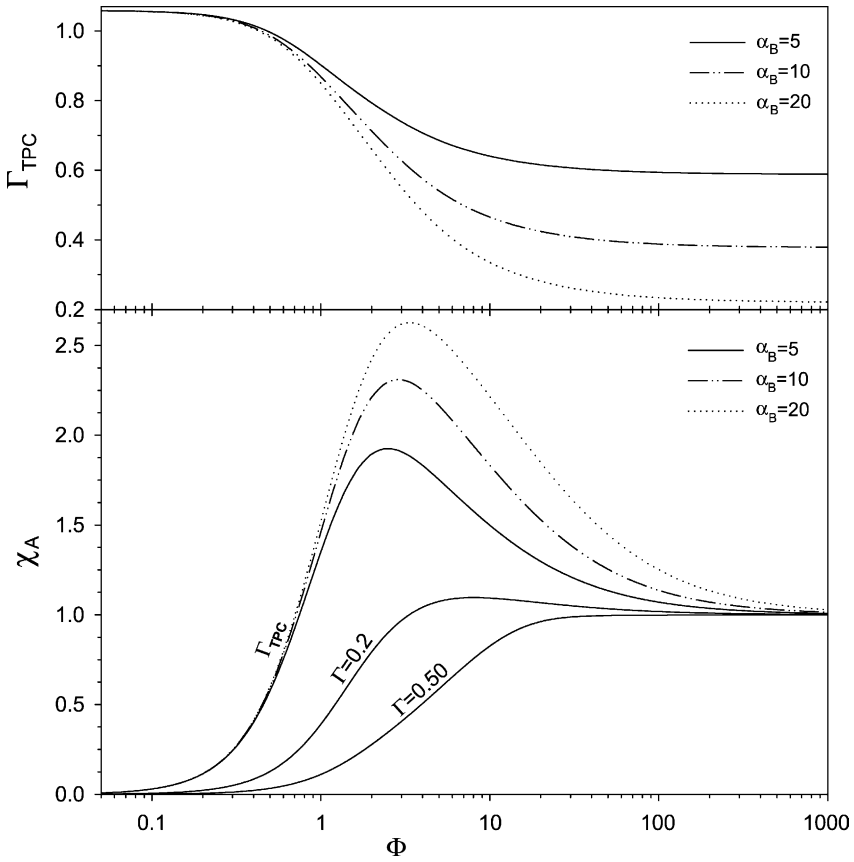

Fig. 2. Upper part: contact time at the TPC as a function of the Thiele modulus for different α_B values. Lower part: relative conversion as a function of the Thiele modulus for different α_B and contact time values ($\alpha_A = 1$, $\gamma_i = 1$, $\Psi_A^F = 1$, $\Psi^R = 1$, $\Psi^P = 0.1$, $r^t/\delta = 10$, $j = 0$, $f = 1$ and $K_e = 0.25$).

sorption coefficient of the reaction product and the reactant. However, the improvement in the conversion penalizes considerably the reactor size, which is proportional to the contact time. So, there should be an optimal contact time for such cases.

This figure shows also that the maximum conversion is now reached for a contact time (Γ_{MC}) lower than the one at TPC, in opposition to the previous case (see Fig. 3, lower part). This results from the combination of the reactant's permeation rate and the reaction rate effects [39]. Working in this region of contact time values could be advantageous from the strict point of view of maximizing the conversion, but has the disadvantage of losing a fraction of reactants that leaves the reactor with the retentate stream.

3.3. Influence of the permeate flow operation

When working with only gas separation, the counter-current flow is better than the co-current one with respect to permeate enrichment or product recovery, leading the cross-flow to an intermediate performance level with respect to the same variables [40]. However, when a chemical reaction takes place inside the selective polymeric catalytic membrane, the results are different. Fig. 4 shows the relative conversion of the reactor as a function of the Thiele modulus, for different contact times and for counter-current, co-current and cross-flow operation modes (lower part) as well as the contact time at the TPC as a function of the Thiele modulus and for the same operation modes (upper part). These results are reported for $\alpha_B > 1$, but the conclusions are still the same whichever is the relative value of the sorption and diffusion coefficients. As it can be seen from this figure, the co-current operation mode is the best and the counter-current is the worst. It can also be seen from this figure that, for the different operation modes, the differences in the reactor performance are relevant only for a medium/high contact times and for an intermediate Thiele modulus range. For low contact times, the net result depends almost exclusively on the retentate composition and flow rate and the flow configuration has almost no influence. For $\Phi \to \infty$, the chemical reaction tends to be in equilibrium throughout all the membrane, resulting in a limited conversion equal to the thermodynamic equilibrium one.

The higher efficiency of the counter-current operation mode when there is only gas separation is the result of a better exploitation of the pressure gradients between the tube and shell sides along the fiber length, as also happens in other processes in chemical engineering (e.g. heat transfer). However, for a catalytic membrane reactor like the one in this study, the partial fluxes through the membrane are not

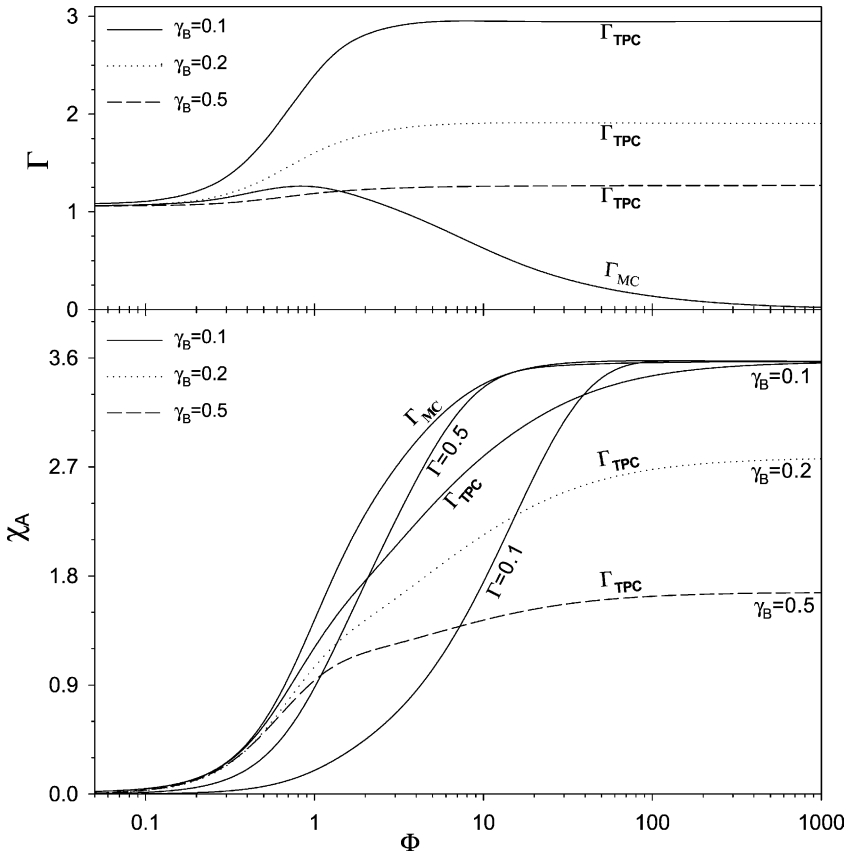

Fig. 3. Upper part: contact time at the TPC and at the maximum conversion as a function of the Thiele modulus for different γ_B values. Lower part: relative conversion as a function of the Thiele modulus for different γ_B and contact time values ($\alpha_i = 1$, $\gamma_A = 1$, $\Psi_A^F = 1$, $\Psi^R = 1$, $\Psi^P = 0.1$, $r^t/\delta = 10$, $j = 0$, $f = 1$ and $K_e = 0.25$).

constant. As can be seen in Figs. 5 and 6, the main changes in the composition profiles of the reaction components, either in the retentate side (Fig. 5) or in the permeate side (Fig. 6), tend to be localized in a progressively shorter region at the reactor's feed side end, as the Thiele modulus values increases. In this way, the performance of the reactor depends essentially on what happens in this region. For co-current or cross-flow operation modes, the pressure of component B on the permeate side at the reactor's feed side end is the minimum possible (the shell side inlet is closed), thus allowing the production of component B inside the membrane to be maximized. For counter-current flow, on the other hand, the concentration of the reaction product in such region is higher than for co-current flow, as a result of the production earlier on (i.e. for higher axial coordinate). This high concentration leads to a back diffusion of component B to the membrane, as it can be observed by the slight decreasing of its partial pressure in Fig. 6.

The magnitude of the conversion differences for these three flow patterns depends on the total pressure gradient between the tube and the shell sides. As the relative permeate pressure decreases ($\Psi^P \rightarrow 0$), the reactor's conversion becomes not influenced by the flow operation mode, because the difference between the partial pressure gradient of the reaction components as a function of the flow operation mode tends to disappear. The existence of a maximum in the concentration of component B in the permeate side for an intermediate Thiele modulus value (see Fig. 6) is related to the maximum of the separation effect, owing to the higher diffusion coefficient of component B [39].

3.4. Influence of the total pressure gradient

Figs. 7 and 8 show the relative conversion and the contact time at the TPC as a function of the Thiele modulus and for different total permeate pressures. Fig. 7 reports for $\alpha_B > 1$ and Fig. 8 reports for $\gamma_B < 1$. The first main conclusion from these two figures is that the contact time for the maximum conversion, whichever is the Thiele modulus, increases with the decreasing of the total pressure gradient. This was expected, because the transport of the reaction components through the membrane depends on their concentration gradients. The second important conclusion concerns the conversion evolution, whose pattern depends exclusively on the permeability of the reaction components [39]. On one hand, the maximum attainable conversion for a higher diffusion coefficient of component B, which takes place for an intermediate Thiele modulus range, decreases with the total

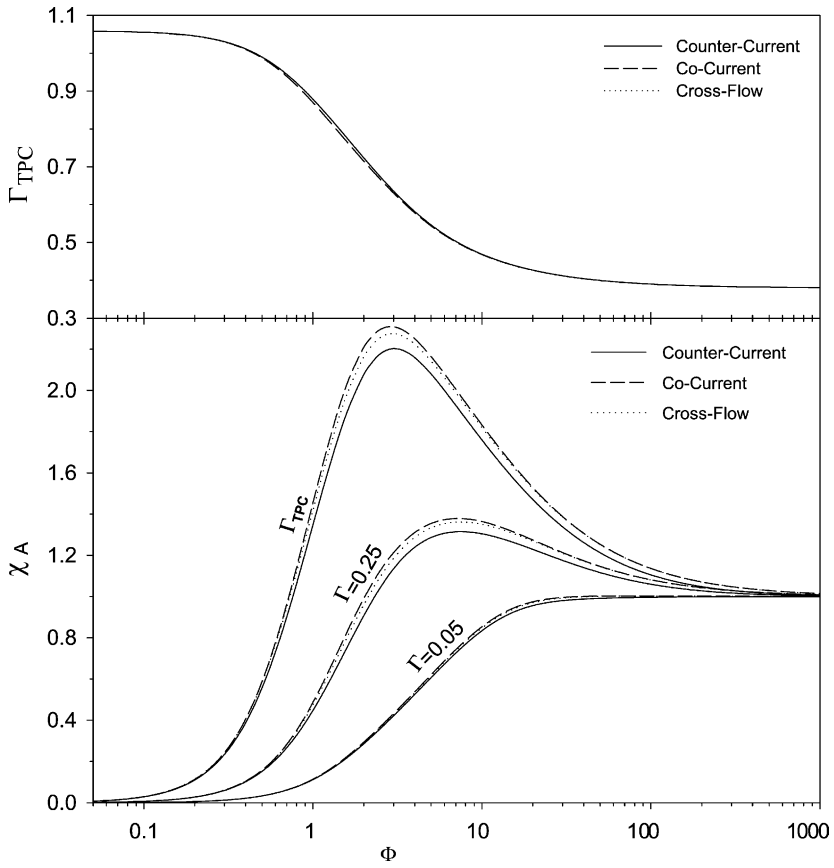

Fig. 4. Upper part: contact time at the TPC as a function of the Thiele modulus for different flow operations. Lower part: relative conversion as a function of the Thiele modulus for different flow operations and contact time values ($\alpha_A = 1$, $\alpha_B = 10$, $\gamma_i = 1$, $\Psi_A^F = 1$, $\Psi^R = 1$, $\Psi^P = 0.1$, $r^t/\delta = 10$, $j = 0$ and $K_e = 0.25$).

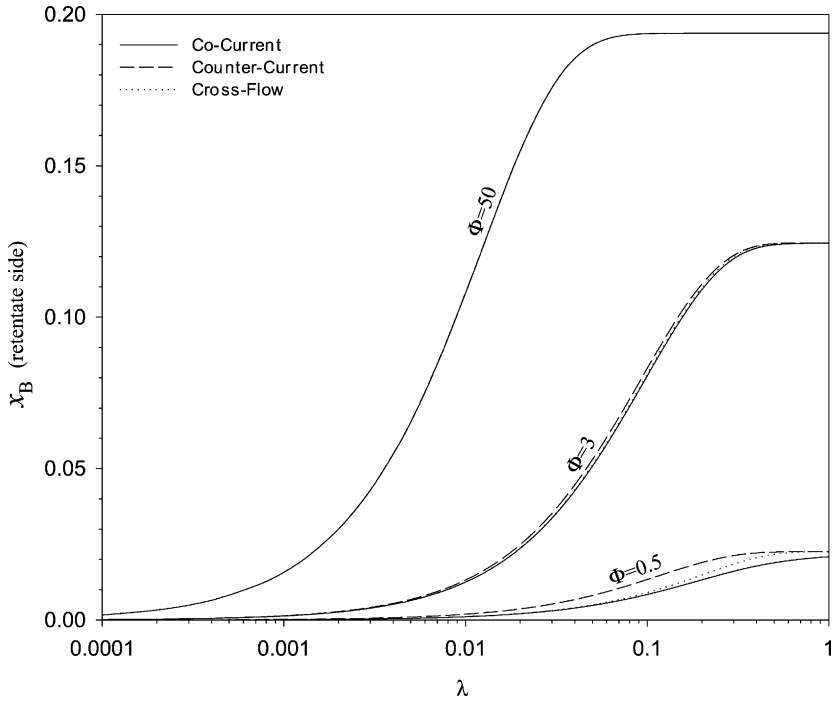

Fig. 5. Molar fractions of the component B in the retentate flow as a function of the axial coordinate, at the TPC and for different Thiele modulus values and flow operations ($\alpha_A = 1$, $\alpha_B = 10$, $\gamma_i = 1$, $\Psi_A^F = 1$, $\Psi^R = 1$, $\Psi^P = 0.1$, $r^t/\delta = 10$, $\Gamma = \Gamma_{TPC}$, $j = 0$ and $K_e = 0.25$).

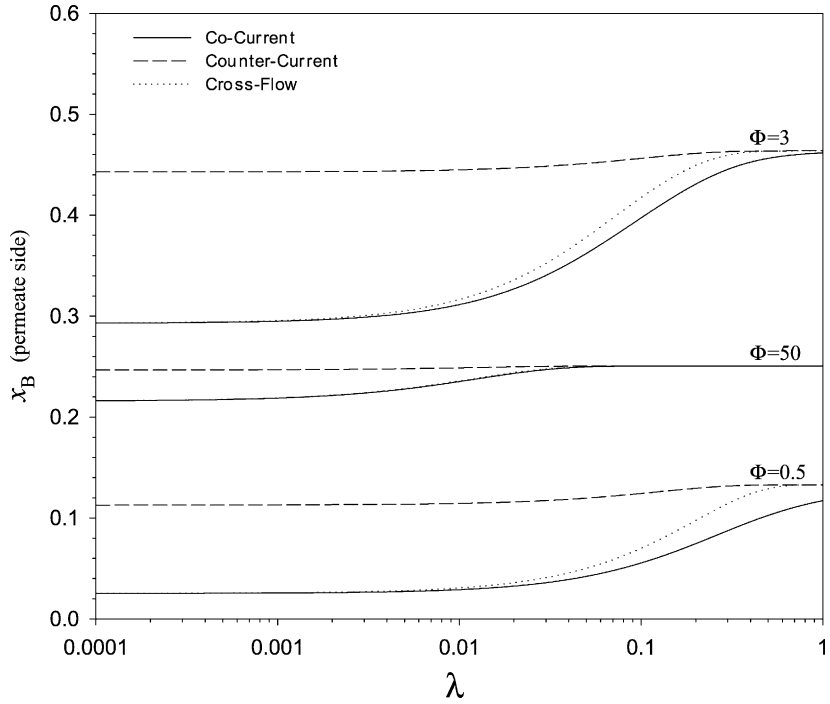

Fig. 6. Molar fractions of the component B in the permeate flow as a function of the axial coordinate, at the TPC and for different Thiele modulus values and flow operations ($\alpha_A = 1$, $\alpha_B = 10$, $\gamma_i = 1$, $\Psi_A^F = 1$, $\Psi^R = 1$, $\Psi^P = 0.1$, $r^t/\delta = 10$, $\Gamma = \Gamma_{TPC}$, $j = 0$ and $K_e = 0.25$).

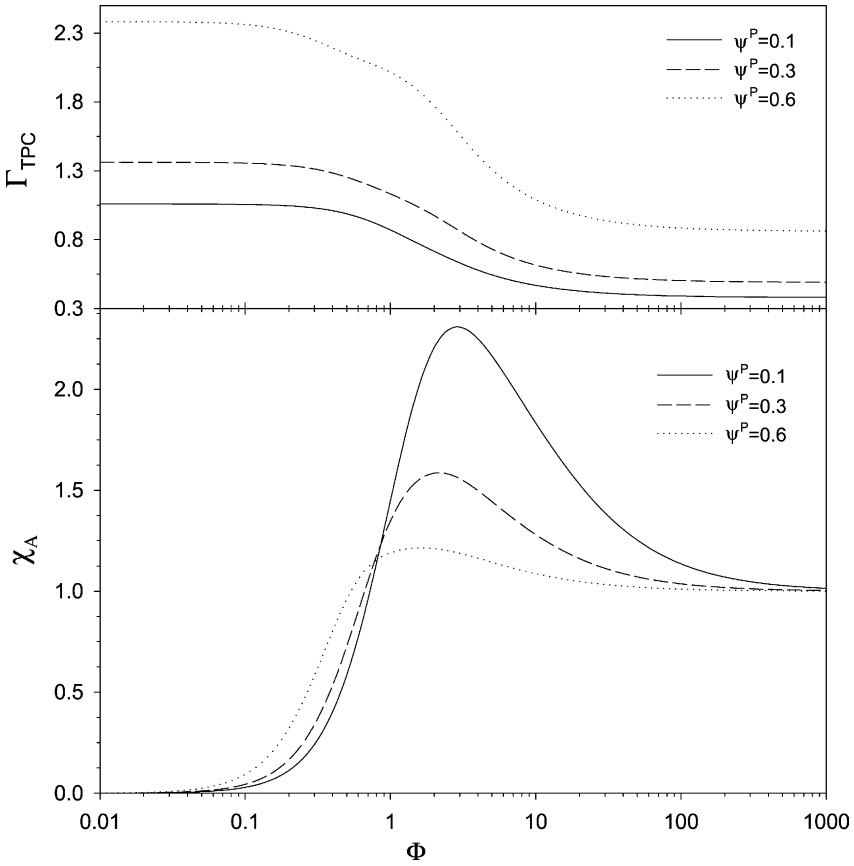

Fig. 7. Relative conversion (lower part) and contact time at the TPC (upper part) as a function of the Thiele modulus for different dimensionless permeate pressure values ($\alpha_A = 1$, $\alpha_B = 10$, $\gamma_i = 1$, $\Psi_A^F = 1$, $\Psi^R = 1$, $r^t/\delta = 10$, $\Gamma = \Gamma_{TPC}$, $j = 0$, $f = 1$ and $K_e = 0.25$).

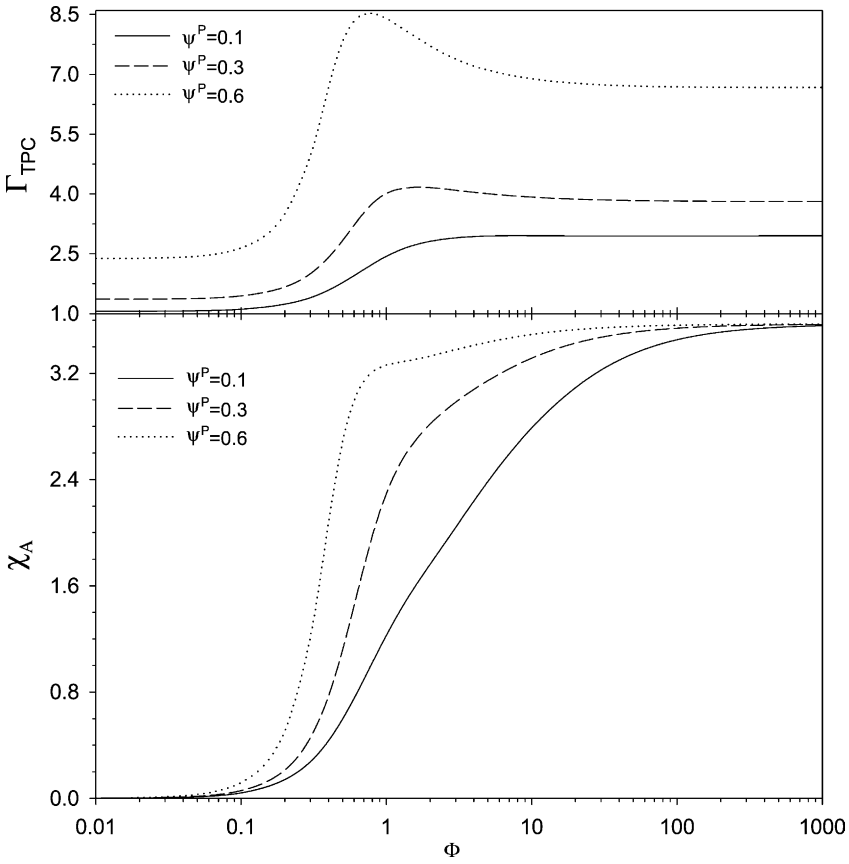

Fig. 8. Relative conversion (lower part) and contact time at the TPC (upper part) as a function of the Thiele modulus for different dimensionless permeate pressure values ($\alpha_i = 1$, $\gamma_A = 1$, $\gamma_B = 0.1$, $\Psi_A^F = 1$, $\Psi^R = 1$, $r^t/\delta = 10$, $\Gamma = \Gamma_{TPC}$, $j = 0$, $f = 1$ and $K_e = 0.25$).

pressure gradient (see Fig. 7). For this case, the enhancement of the conversion is a direct consequence of the preferential transport of the reaction product through the membrane, the 'separation effect' [39]. In this way, the reactor conversion is directly connected with the total gradient pressure through the membrane. As the total permeate pressure approaches the retentate one, the separation effect is getting more and more offset and the maximum conversion tends towards the thermodynamic equilibrium one. For a lower sorption coefficient of component B (see Fig. 8), the main differences in the reactor's conversion as a function of the Thiele modulus occur also for an intermediate range of this parameter (Thiele modulus). However, the conversion increases now with the decrease of the total pressure gradient, for a given Thiele modulus value, also as a consequence of the separation effect: the higher permeability of the reactants through the membrane penalizes the conversion [39]. In this way, a decreasing driving force through the membrane decreases the influence of the separation effect, leading to an increase of the conversion. On the other hand, the limit conversion ($\Phi \rightarrow \infty$) attained for both cases does not change with the permeate pressure (see Figs. 7 and 8). In such cases, any separation effect is completely offset, as the chemical reaction is in equilibrium throughout all the membrane. The limit conversion depends only on the relative sorption coefficients of the reaction components: a lower sorption for the reaction product enhances the conversion relative to the thermodynamic equilibrium value (see Fig. 8); on the other hand, an equal sorption for all components does not have any effect on the conversion (see Fig. 7); a higher sorption for the reaction product penalizes the conversion [39].

The evolution of the contact time at the TPC as a function of the Thiele modulus for both cases (Figs. 7 and 8) is a net result of the balance between the conversion evolution (which affects the contact time, as a result of the average permeability for the reaction components is changing) and the evolution of the displacement of the equilibrium fronts inside the membrane towards its surfaces (which affects the reaction components residence time inside the membrane) [39].

3.5. Influence of the feed location (tube side or shell side) and the r^t/δ ratio

Fig. 9 shows the relative conversion (lower part) and the contact time at the TPC (upper part) as a function of the Thiele modulus for $\alpha_B > 1$, for different ratios between the tube radius and the membrane thickness (r^t/δ) and for both tube and shell side feed. As can be seen, the location of the reactor feed at the shell side is always better than at the tube

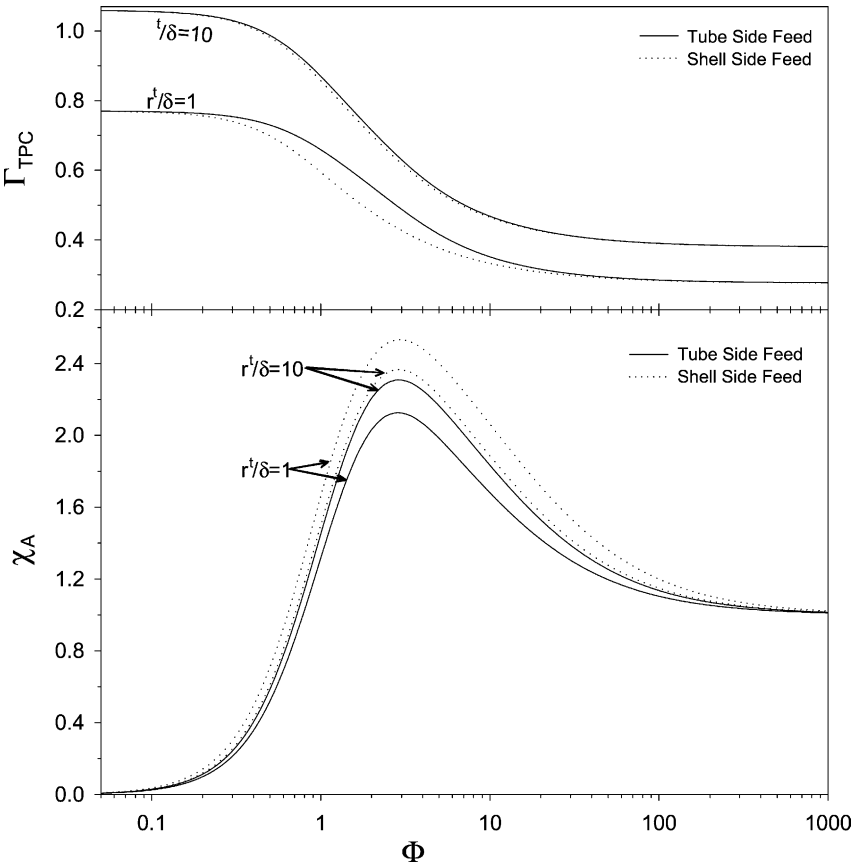

Fig. 9. Relative conversion (lower part) and contact time at the TPC (upper part) as a function of the Thiele modulus for different feed locations and r^t/δ ratios ($\alpha_A = 1$, $\alpha_B = 10$, $\gamma_i = 1$, $\Psi_A^F = 1$, $\Psi^R = 1$, $\Psi^P = 0.1$, $\Gamma = \Gamma_{TPC}$, $f = 1$, and $K_e = 0.25$).

side, concerning the reactor conversion. These results still show that, for the tube side feed, the conversion increases with the r^t/δ ratio, while a reverse relation is observed for the shell side feed. Such trends are a direct consequence of the membrane's cylindrical geometry. For a high r^t/δ ratio (membrane approaching the flat shape), the membrane area is nearly constant as a function of the radial coordinate and the influence of the feed location (tube or shell side) is negligible (see Figs. 9 and 10). But as the r^t/δ ratio decreases, the membrane area varies more and more with the radial coordinate, leading to a favorable or unfavorable impact on the reaction components concentration. For the tube side feed, both the chemical reaction and membrane's cylindrical geometry, which area increases with the radial co-ordinate, contribute to decrease the reactant concentration, leading in this way to a conversion penalization. When the reactor is fed from the shell side, on the other hand, decreasing of the area as the reactants proceeds through the membrane lessens the impact of the chemical reaction on the reactant concentration, keeping it higher and enhancing the conversion in this way (see Figs. 9 and 10).

For each r^t/δ, the differences on the contact time with respect to the feed location (see Fig. 9, upper part) are a consequence of the different attained conversions (component B is the faster one). This figure still shows an increase of the contact time with the r^t/δ ratio. However, such a comparative analyze is not straightforward, because the value of r^t is different in both cases (the change on the r^t/δ ratio with constant Thiele modulus implies a change on r^t for δ constant).

The former results are concerned to the case where the diffusion coefficient of the reaction product is higher than the reactant one. However, they might be extended to a general case where the reaction product permeability is higher than the reactant one. On one hand, the separation effect leads to an enhancement of the conversion for intermediate range of Thiele modulus values. On the other hand, the decreasing of the membrane area as a function of the radial coordinate when the reactor is fed from the shell side keeps the concentration of the reactant (the slowest component) higher than when the reactor is fed from the tube side.

When the reactant permeability is higher than the reaction product one, on the other hand, the conclusions are different. It was shown in Fig. 3 that, for a given Thiele modulus value belonging to the intermediate range, the reactor conversion increases with the contact time until a value where the conversion reaches its maximum value (Γ_{MC}) and then decreases until the total permeation condition (Γ_{TPC}). Although these results have been obtained for $\gamma_B < 1$, the conclusions are kept for a general case when the permeability of the reaction product is lower than the reactant one. Fig. 11

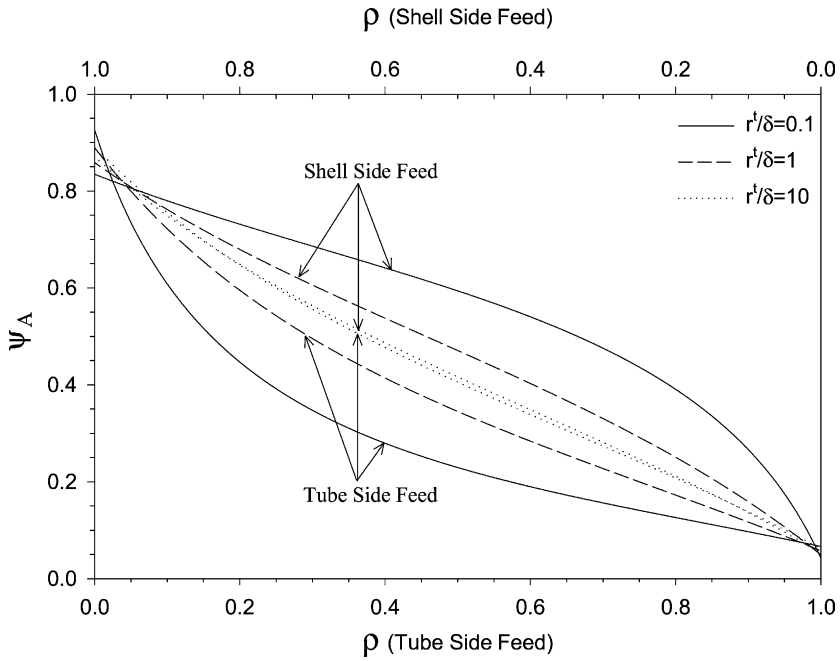

Fig. 10. Dimensionless partial pressure of the component B inside the membrane (Ψ_B) for different feed locations and r^t/δ ratios ($\alpha_A = 1$, $\alpha_B = 10$, $\gamma_i = 1$, $\Psi_A^F = 1$, $\Psi^R = 1$, $\Psi^P = 0.1$, $\Gamma = \Gamma_{TPC}$, $\Phi = 3$, $\lambda = 1$, $f = 1$, and $K_e = 0.25$).

shows the influence of the feed location (tube or shell side) on the reactor's conversion as a function of the contact time, for a few Thiele modulus values and for $\gamma_B < 1$. Contrary to the previous case, the best feed location (with respect to the conversion) depends now on the Thiele modulus and the contact time values. For low Thiele modulus values, the shell side feed is better than the tube side one, whichever is the contact time. For medium/high Thiele modulus values, the shell side feed is better than the tube side feed only for contact times lower than the one for the maximum conversion (Γ_{MC}). As in the previous case, these results are a consequence of the membrane's cylindrical geometry. When $\Gamma < \Gamma_{MC}$, the reaction occurs in the forward direction [39], and like for the case where the permeability of component B is higher, the shell side feed location favors the conversion. For $\Gamma > \Gamma_{MC}$, the backward reaction is the dominant one [39]. In this way, the enhancement of the component's B concentration leads to a higher decrease in the conversion.

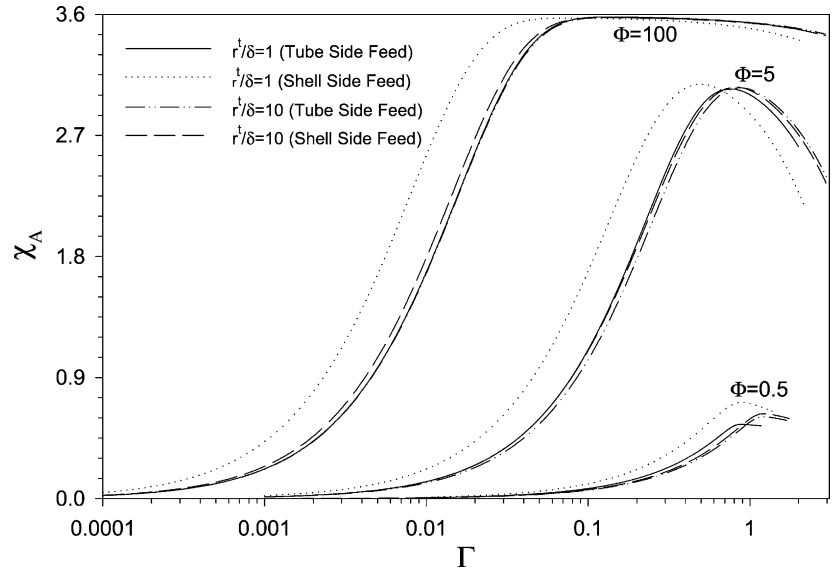

Fig. 11. Relative conversion as a function of the contact time for different feed locations, Thiele modulus and r^t/δ ratios ($\alpha_i = 1$, $\gamma_A = 1$, $\gamma_B = 0.1$, $\Psi_A^F = 1$, $\Psi^R = 1$, $\Psi^P = 0.1$, $f = 1$, and $K_e = 0.25$).

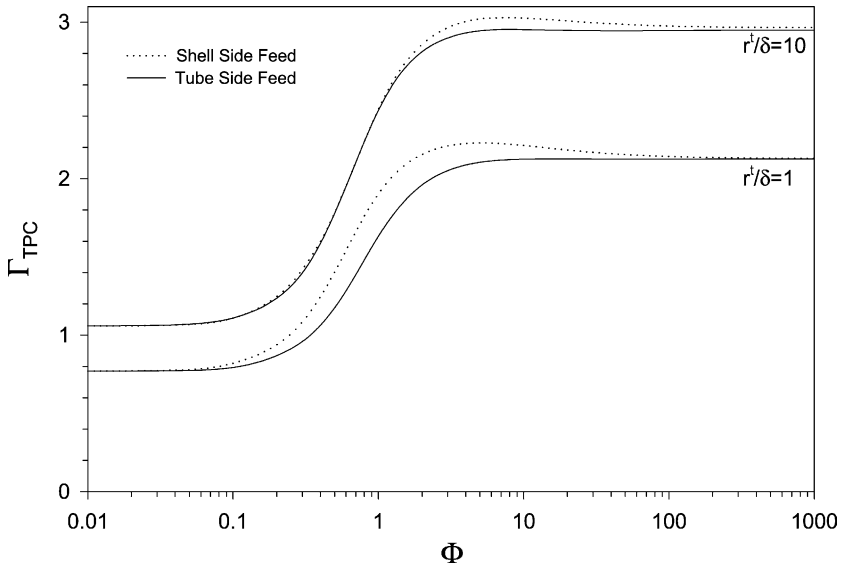

Fig. 12. Contact time at the TPC as a function of the Thiele modulus for different feed locations and r^t/δ ratios ($\alpha_i = 1$, $\gamma_A = 1$, $\gamma_B = 0.1$, $\Psi_A^F = 1$, $\Psi^R = 1$, $\Psi^P = 0.1$, $f = 1$, and $K_e = 0.25$).

Fig. 11 still shows that the influence of the feed location on the conversion becomes irrelevant as the membrane tends to the flat shape.

Fig. 12 shows that the enhancement of the component B concentration for a shell side feed leads to a higher contact time at the TPC, because this component is the slowest (for the same r^t/δ ratio). As in the previous case, the differences between the contact time at the TPC for different r^t/δ ratios are not comparable.

4. Conclusions

In the present study, we analyzed a dense polymeric catalytic membrane reactor operating in isothermal conditions. An equilibrium-limited gas phase generic reaction of the type A⇄ B was considered for the reason that an analytical solution for the mass balance equations for the membrane can be written. A study was made on the influence that some parameters and operation modes have in the reactor's conversion. The results presented showed that, for a given set of conditions, it is possible to obtain conversions well above the thermodynamic value, as for example, when the reaction products have a lower sorption coefficient and/or a higher diffusion coefficient than the reactants one. It was also shown that: the co-current flow is always better than the counter-current flow; the relative permeate pressure could favor or penalize the conversion, depending on the permeabilities of each component, and the contact time at the TPC increases as the total pressure gradient across the membrane decreases; the best reactor's feed location and the optimum r^t/δ ratio depend on the relative sorption and diffusion coefficients of the reaction components as well as on the range of the Thiele modulus and contact time values. Although it was not considered in the present study, the pressure drop should be taken into account whenever it becomes relevant, as for example, for membranes with very low internal diameter and/or high length or when the velocity of the retentate stream is high.

Acknowledgements

The authors acknowledge the research project Sapiens 32452/99 funded by FCT.

Appendix A

In this section, the analytical solution for the membrane mass balance equations is presented. Let us consider Eq. (15), which represents the membrane mass balances. Making the variable substitution $\sigma = \rho + (r^t/\delta)$, these two differential equations could be represented in the matrix form as it follows:

$$\frac{d^2\bar{\Psi}}{d\sigma^2} + \frac{1}{\sigma}\frac{d\bar{\Psi}}{d\sigma} - \mathbb{A}\bar{\Psi} = 0 \tag{A.1}$$

where $\bar{\Psi}$ represents the vector of dependent variables, $\begin{bmatrix} \Psi_A \\ \Psi_B \end{bmatrix}$, and the matrix $\mathbb{A}$ is given by:

$$\mathbb{A} = \begin{bmatrix} \dfrac{\Phi^2\gamma_A}{\alpha_A\gamma_A} & -\dfrac{\Phi^2\gamma_B}{\alpha_A\gamma_A K_e} \\ -\dfrac{\Phi^2\gamma_A}{\alpha_B\gamma_B} & \dfrac{\Phi^2\gamma_B}{\alpha_B\gamma_B K_e} \end{bmatrix}.$$

Considering that component A is the reference one, α_A and γ_A are unitary and matrix $\mathbb{A}$ is further simplified:

$$\mathbb{A} = \begin{bmatrix} \Phi^2 & -\dfrac{\Phi^2\gamma_B}{K_e} \\ -\dfrac{\Phi^2}{\alpha_B\gamma_B} & \dfrac{\Phi^2}{\alpha_B K_e} \end{bmatrix}.$$

Eq. (A.1) can be transformed in a Bessel equation. However, the respective solution cannot be obtained directly, as matrix $\mathbb{A}$ is singular. In this way, the system of two equations represented in (A.1) should be further transformed in two another linearly independent equations as follows:

$$\begin{cases} \dfrac{d^2\Upsilon_A}{d\sigma^2} + \dfrac{1}{\sigma}\dfrac{d\Upsilon_A}{d\sigma} = 0 \\ \dfrac{d^2\Upsilon_B}{d\sigma^2} + \dfrac{1}{\sigma}\dfrac{d\Upsilon_B}{d\sigma} - \Phi^2\left(1 + \dfrac{1}{\alpha_B K_e}\right)\Upsilon_B = 0 \end{cases} \tag{A.2}$$

with

$$\begin{bmatrix} \Upsilon_A \\ \Upsilon_B \end{bmatrix} = \begin{bmatrix} \dfrac{1}{1+\alpha_B K_e} & \dfrac{\alpha_B\Upsilon_B}{1+\alpha_B K_e} \\ \dfrac{\alpha_B K_e}{1+\alpha_B K_e} & -\dfrac{\alpha_B\gamma_B}{1+\alpha_B K_e} \end{bmatrix} \begin{bmatrix} \Psi_A \\ \Psi_B \end{bmatrix}$$

The solution for the first equation of (19) is:

$$\Upsilon_A = C_1 + C_2 \ln(\sigma) \tag{A.3}$$

The second equation of (19) can be transformed in a modified Bessel equation of order 0, after making the substitutions $\Phi^2\,(1 + (1/\alpha_B K_e)) = \eta^2$ and $\eta^2\sigma^2 = \omega^2$:

$$\omega^2\frac{d^2\Upsilon_B}{d\omega^2} + \omega\frac{d\Upsilon_B}{d\omega} - \omega^2\Upsilon_B = 0 \tag{A.4}$$

The solution of this equation is a combination of the Bessel functions $I_0(\omega)$ and $K_0(\omega)$ as follows:

$$\Upsilon_B = C_3 I_0(\omega) + C_4 K_0(\omega) \tag{A.5}$$

The solution for the initial system of equations (Eq. (15)) is then:

$$\begin{bmatrix} \Psi_A \\ \Psi_B \end{bmatrix} = (C_1 + C_2\ln\sigma)\begin{bmatrix} 1 \\ \dfrac{K_e}{\gamma_B} \end{bmatrix} + C_3\begin{bmatrix} 1 \\ -\dfrac{1}{\alpha_B\gamma_B} \end{bmatrix} I_0(\omega) + C_4\begin{bmatrix} 1 \\ -\dfrac{1}{\alpha_B\gamma_B} \end{bmatrix} K_0(\omega),$$

with the constants C_1–C_4 given by the following expressions:

$$C_1 = \frac{(\Psi_A^P(\lambda) + \alpha_B\gamma_B\Psi_B^P(\lambda))\ln(\delta/r^t) + (\Psi_A^R(\lambda) + \alpha_B\gamma_B\Psi_B^R(\lambda))\ln(1 + (r^t/\delta))}{(1+\alpha_B K_e)\ln(1 + (\delta/r^t))}$$

$$C_2 = \frac{\Psi_A^P(\lambda) - \Psi_A^R(\lambda) + \alpha_B\gamma_B(\Psi_B^P(\lambda) - \Psi_B^R(\lambda))}{(1+\alpha_B K_e)\ln(1 + (\delta/r^t))}$$

$$C_3 = \frac{\begin{array}{c}(\alpha_B K_e\Psi_A^R(\lambda) - \alpha_B\gamma_B\Psi_B^R(\lambda))K_0(\eta(1 + (\delta/r^t))) \\ -(\alpha_B K_e\Psi_A^P(\lambda) - \alpha_B\gamma_B\Psi_B^P(\lambda))K_0(\eta\delta/r^t)\end{array}}{\begin{array}{c}(1+\alpha_B K_e)[I_0(\eta\delta/r^t)K_0(\eta(1 + (\delta/r^t))) \\ -I_0(\eta(1 + (\delta/r^t)))K_0(\eta\delta/r^t)]\end{array}}$$

$$C_4 = -\frac{\begin{array}{c}(\alpha_B K_e\Psi_A^R(\lambda) - \alpha_B\gamma_B\Psi_B^R(\lambda))I_0(\eta(1 + (\delta/r^t))) \\ -(\alpha_B K_e\Psi_A^P(\lambda) - \alpha_B\gamma_B\Psi_B^P(\lambda))I_0(\eta\delta/r^t)\end{array}}{\begin{array}{c}(1+\alpha_B K_e)[I_0(\eta\delta/r^t)K_0(\eta(1 + (\delta/r^t))) \\ -I_0(\eta(1 + (\delta/r^t)))K_0(\eta\delta/r^t)]\end{array}}$$

References

[1] K.K. Sirkar, P.V. Shanbhag, A.S. Kovvali, Membrane in a reactor: a functional perspective, Ind. Eng. Chem. Res. 38 (1999) 3715.

[2] J. Sanchez, T.T. Tsotsis, Current developments and future research in catalytic membrane reactors, in: A.J. Burggraaf, L. Cot (Eds.), Fundamentals of Inorganic Science and Technology, Elsevier, Amsterdam, 1996, pp. 529–568.

[3] J.S. Marcano, T.T. Tsotsis, Catalytic Membranes and Membrane Reactors, Wiley–VCH Verlag GmbH, Weinheim, 2002.

[4] G. Saracco, H.W.J.P. Neomagus, G.F. Versteeg, W.P.M. van Swaaij, High-temperature membrane reactors: potential and problems, Chem. Eng. Sci. 54 (1999) 1997.

[5] G. Saracco, J.W. Veldsink, G.F. Versteeg, W.P.M. van Swaaij, Catalytic combustion of propane in a membrane reactor with separate feed of reactants. Part II. Operation in the presence of trans-membrane pressure gradients, Chem. Eng. Sci. 50 (1995) 2833.

[6] H.W.J.P. Neomagus, G. Saracco, H.F.W. Wessel, G.F. Versteeg, The catalytic combustion of natural gas in a membrane reactor with separate feed of reactants, Chem. Eng. J. 77 (2000) 165.

[7] M.P. Harold, C. Lee, Intermediate product yield enhancement with a catalytic inorganic membrane. Part II. Non-isothermal and integral operation in a back-mixed reactor, Chem. Eng. Sci. 52 (1997) 1923.

[8] F.A. Al-Sherehy, A.M. Adris, M.A. Soliman, R. Hughes, Avoidance of flammability and temperature runaway during oxidative dehydrogenation using a distributed feed, Chem. Eng. Sci. 53 (1998) 3695.

[9] S.-I. Niwa, M. Eswaramoorthy, J. Nair, A. Raj, N. Itoh, H. Shoji, T. Namba, F. Mizukami, A one-step conversion of benzene to phenol with a palladium membrane, Science 295 (2002) 105.

[10] V. Diakov, A. Varma, Reactant distribution by inert membrane enhances packed-bed reactor stability, Chem. Eng. Sci. 57 (2002) 1099.

[11] Y. Lu, A.G. Dixon, W.R. Moser, Y.H. Ma, U. Balachandran, Oxygen-permeable dense membrane reactor for the oxidative coupling of methane, J. Membr. Sci. 170 (2000) 27.

[12] H. Weyten, J. Luyten, K. Keizer, L. Willems, R. Leysen, Membrane performance: the key issues for dehydrogenation reactions in a catalytic membrane reactor, Catal. Today 56 (2000) 3.

[13] J. Shu, B.P.A. Grandjean, A. van Neste, S. Kaliaguine, Catalytic palladium-based membrane reactors—a review, Can. J. Chem. Eng. 69 (1991) 1036.

[14] N. Itoh, T-H. Wu, An adiabatic type of palladium membrane reactor for coupling endothermic and exothermic reactions, J. Membr. Sci. 124 (1997) 213.

[15] R. Dittmeyer, V. Höllein, K. Daub, Membrane reactors for hydrogenation and dehydrogenation processes based on supported palladium, J. Mol. Cat. Part A. Chem. 173 (2001) 135.

[16] A.M. Champagnie, T.T. Tsotsis, R.G. Minet, E. Wagner, The study of ethane dehydrogenation in a catalytic membrane reactor, J. Catal. 134 (1992) 713.
[17] H. Weyten, K. Keizer, A. Kinoo, J. Luyten, R. Leysen, Deydrogenation of propane using a packed-bed catalytic membrane reactor, AIChE J. 43 (1997) 1819.
[18] T. Brinkmann, S.P. Perera, W.J. Thomas, Membrane catalysis, Chem. Eng. Sci. 56 (2001) 2047.
[19] E. Gobina, R. Hughes, Ethane dehydrogenation using a high temperature catalytic membrane reactor, J. Membr. Sci. 90 (1994) 11.
[20] E. Gobina, K. Hou, R. Hughes, Ethane dehydrogenation in a catalytic membrane reactor coupled with a reactive sweep gas, Chem. Eng. Sci. 50 (1995) 2311.
[21] M.E. Rezac, W.J. Koros, S.J. Miller, Membrane-assisted dehydrogenation of *n*-butane: influence of membrane properties on system performance, J. Membr. Sci. 93 (1994) 193.
[22] I.F.J. Vankelecom, K.A.L. Vercruysse, P.E. Neys, D.W.A. Tas, K.B.M. Janssen, P.-P. Knops-Gerrits, P.A. Jacobs, Novel catalytic membranes for selective reactions, Top. Catal. 5 (1998) 125.
[23] S. Tennison, Current hurdles in the commercial development of inorganic membrane reactor, in: Proceedings of the Fourth International Conference on Catalysis in Membrane Reactors, Zaragoza, Spain, 3–5 July 2000, pp. 13–17.
[24] D. Fritsch, K.-V. Peinemann, Novel highly permselective 6F-poly(amide–imide)s as membrane host for nano-sized catalysts, J. Membr. Sci. 99 (1995) 29.
[25] J.F. Ciebien, R.E. Cohen, A. Duran, Catalytic properties of palladium nanoclusters synthesized within diblock copolymer films: hydrogenation of ethylene and propylene, Supramol. Sci. 5 (1998) 31.
[26] J. Vital, A.M. Ramos, I.F. Silva, H. Valente, J.E. Castanheiro, Hydration of α-pinene over zeolites and activated carbons dispersed in polymeric membranes, Catal. Today 56 (2000) 167.
[27] G. Langhendries, G.V. Baron, I.F.J. Vankelecom, R.F. Parton, P.A. Jacobs, Selective hydrocarbon oxidation using a liquid-phase catalytic membrane reactor, Catal. Today 56 (2000) 131.
[28] I.F.J. Vankelecom, P.A. Jacobs, Dense organic catalytic membranes for fine chemical synthesis, Catal. Today 56 (2000) 147.
[29] P.E.F. Neys, A. Severeyns, I.F.J. Vankelecom, E. Ceulemans, W. Dehaen, P.A. Jacobs, Manganese porphyrins incorporated in PDMS: selective catalysts for the epoxidation of deactivated alkenes, J. Mol. Catal. 144 (1999) 373.
[30] W.J. Koros, R.T. Chern, Separation of gaseous mixtures using polymer membranes, in: R.W. Rousseau (Ed.), Handbook of Separation Process Technology, Wiley, New York, 1987, pp. 862–953.
[31] A.A. Yawalker, V.G. Pangarkar, G.V. Baron, Alkene epoxidation with peroxide in a catalytic membrane reactor: a theoretical study, J. Membr. Sci. 182 (2001) 129.
[32] J.M. Sousa, P. Cruz, A. Mendes, Modeling a catalytic polymeric non-porous membrane reactor, J. Membr. Sci. 181 (2001) 241.
[33] J.M. Sousa, P. Cruz, A. Mendes, A study on the performance of a dense polymeric catalytic membrane reactor, Catal. Today 67 (2001) 281.
[34] J. Vital, A.M. Ramos, I.F. Silva, H. Valente, J.E. Castanheiro, The effect of α-terpineol on the hydration of α-pinene over zeolites dispersed in polymeric membranes, Catal. Today 67 (2001) 217.
[35] S. Wu, J.-E. Gallot, M. Bousmina, C. Bouchard, S. Kaliaguine, Zeolite containing catalytic membranes as interphase contactors, Catal. Today 56 (2000) 113.
[36] A.M. Champagnie, T.T. Tsotsis, R.G. Minet, E. Wagner, The study of ethane dehydrogenation in a catalytic membrane reactor, J. Catal. 134 (1992) 713.
[37] M.J. Thundyil, W.J. Koros, Mathematical modeling of gas separation permeators for radial cross flow, counter-current and co-current hollow-fiber membrane modules, J. Membr. Sci. 125 (1997) 275.
[38] L.R. Petzold, A.C. Hindmarsh, LSODA, Computing and Mathematics Research Division, Lawrence Livermore National Laboratory, 1997.
[39] J.M. Sousa, A. Mendes, Modeling a dense polymeric catalytic membrane reactor with plug–flow pattern, Catal. Today, 2003, in press.
[40] C.Y. Pan, Gas separation by permeators with high-flux asymmetric membranes, AIChE J. 29 (1983) 545.